SCIENCE CHINA
Technological Sciences

•Article•

December 2020 Vol.63 No.12: 2518–2526
https://doi.org/10.1007/s11431-020-1741-2

Programmable soft bending actuators with auxetic metamaterials

PAN Qi[1], CHEN ShiTong[1], CHEN FeiFei[1,2*] & ZHU XiangYang[1,2]

[1] *Robotics Institute, School of Mechanical Engineering, Shanghai Jiao Tong University, Shanghai 200240, China;*
[2] *State Key Laboratory of Mechanical System and Vibration, Shanghai Jiao Tong University, Shanghai 200240, China*

Received July 9, 2020; accepted October 26, 2020; published online November 9, 2020

Soft robotics has been receiving increasing attention due to its flexibility and adaptability offered by embodied intelligence. A soft robot may undergo complex motions including stretching, contraction, bending, twisting, and their intricate combinations. Among these basic motions, bending plays a central role when a robot accomplishes tasks such as locomotion, grasping and manipulation. Although a rich repertoire of bending mechanisms has been reported, a systematic and rational design framework is still lack. In this paper, we provide a novel design strategy for soft bending actuators which allows integral modeling and design optimization. Nowadays, metamaterials are emerging as a new tool for soft robots, by encoding the desired complex motions directly within the material architectures, leading to conformable monolithic systems. We combine pneumatic actuators and flexible metamaterials to provide an alternative solution to soft bending actuators, with advantages of compact design, large bending motion, and convenient fabrication. A regular pneumatic chamber is embedded inside auxetic and non-auxetic metamaterials, and bending is generated when inflated. We carry out dimensionless analysis to identify the key design variables. To provide insight into design optimization, we develop a computation framework by modeling metamaterial structures with beam elements and the inner chamber with shell elements as an integral part, allowing efficient simulation of the coupled system. We systematically investigate how the bending angle varies with the key design variables and find the optimal design parameters. The experimental results are well in line with the simulation, and a remarkable bending motion of 0.43°/mm is achieved.

soft robotics, bending actuator, auxetic metamterials, negative Poisson's ratio

Citation: Pan Q, Chen S T, Chen F F, et al. Programmable soft bending actuators with auxetic metamaterials. Sci China Tech Sci, 2020, 63: 2518–2526, https://doi.org/10.1007/s11431-020-1741-2

1 Introduction

In the past decade, the emerging field of soft robotics has been enriching the interpretation of what a robot is and where a robot can be used. The inclusion of soft materials provides a robotic system with unprecedented flexibility and adaptability [1], and thus unlocks potentials for a variety of applications ranging from artificial muscles [2], wearable devices [3,4] and prosthetics [5,6] to search and rescue in unstructured environments [7]. In general, a soft robot with embodied compliance may undergo complex motions including stretching, contraction, bending, twisting, and their intricate combinations. Among these basic motions, the bending mode, as an analog of the revolute joint in conventional rigid robots, plays a key role when a soft robot accomplishes tasks such as locomotion [8,9], grasping [10,11] and manipulation [12].

Many efforts have been made to design and fabrication of soft bending actuators. The key to generating bending is inclusion of asymmetry in terms of the structure of the actuator or the applied external loads, and to date various examples have been reported. From the perspective of geometry, Ilievski et al. [13] delicately designed the shape of channels inside a pneumatic actuator, i.e., the well-known "PneuNets", and the asymmetric channels lead to remarkable bending motions upon pressurization. Yang et al. [14] pro-

*Corresponding author (email: ffchen@sjtu.edu.cn)

posed eccentric soft bending actuators and reinforced the stiffness by surrounding the actuators with stiff fibers.

The selection of materials, coupled with the geometry of the channels, determines the response of the actuator to an applied pressure. The strain-limiting layer made of a relatively harder material and placed on the compression side further shifts the neutral axis and thus promotes the effect of flexure, which represents a multimaterial perspective to induce asymmetry [15,16]. In addition, from the perspective of actuation, eccentric loads from the neutral axis can generate bending moments and lead to bending motions. This is the case in refs. [11,17], where the cable tensions or pressurizations were applied with a distance from the neutral axis.

In a more general sense, the geometric shape or the multimaterial distribution of the actuator can be further optimized. The theory of topology optimization can lend themselves to automatic design of soft actuators and robots [18,19]. Zhang et al. [20,21] optimized the layout of the coating layer of a regular pneumatic tube, using a density-based topology optimization approach, in order to induce maximum bending motions. With the same goal, Chen et al. [11] optimized the layout of a cable-driven bending module for grasping, using a level-set-based topology optimization method. However, these works suffer from the limitation that the material nonlinearities were not incorporated into the optimization model. Besides, the computational cost is typically high, hindering the wide application in customized design of soft actuators.

Despite the reported bending actuators above, they each do not yet represent a universal solution that allows systematic and rational design and convenient fabrication. Nowadays, metamaterials are emerging as a new tool for design of structures and mechanisms, by encoding the desired complex motions directly within the material architectures, leading to conformable monolithic systems [22]. A large category of flexible metamaterials are characterized by cellular structures consisting of slender beams. By carefully arranging elastic beam elements, a variety of unusual mechanical behaviors can be achieved, such as negative Poisson's ratios (auxetics). The incorporation of such metamaterials may imbue soft robots with mechanical intelligence which is hardly attainable with aforementioned conventional design approaches. For instance, the combination of auxetic and non-auxetic clutches simplified a soft robot's three-step locomotion using a single actuator instead of three independent ones [23].

Recently, researchers have made initial attempts to exploration of mechanical metamaterials for building soft bending actuators. Goswami et al. [24] encoded bending within gradient metamaterial structures generated through a Voronoi tessellation algorithm. However, the actuation was limited to tendons and the lightweight design with low stiffness might easily suffer buckling. Starting from the concept of tunable Poisson's ratio, Han and Lu [25] and Hasse and Mauser [26] designed a family of interconnected metamaterial structures that map to a range of Poisson's ratio from positive to negative, and by modulating their distributions bending motions could be readily achieved. However, the design paradigm was limited by the lack of accurate and efficient computation model and simulation tools. A rational design framework is in high demand which not only in general allows freeform metamaterial structure design but also can accurately capture the nonlinear material properties.

In this paper, we combine pneumatic actuators and flexible metamaterials to provide an alternative solution to soft bending actuators, with advantages of compact design, large bending motion, and convenient fabrication. A regular pneumatic chamber is embedded inside auxetic and non-auxetic metamaterials, and bending is generated when inflated. We carry out dimensionless analysis to identify the key design variables, i.e., the geometric aspect ratio of metamaterial structures, and the relative material ratio. To provide insight into design optimization, we develop a computation framework by modelling metamaterial structures with beam elements, based on which we then construct the inner chambers with shell elements to form an integral part, without the need for defining additional interaction constraints. This modelling approach greatly improves the computational convergence and stability, allowing efficient simulation of the coupled system under pressurization. We systematically investigate how the bending angle varies with the key design variables and find the optimal parameters. The experimental results are well in line with the simulation, and a remarkable bending motion of 0.43°/mm is achieved.

The remainder of this paper is organized as follows. Sect. 2 introduces the design concept. Sect. 3 describes the mechanical model for the bending actuator in which the inner rubber is captured by the hyperelastic Neo-Hooke model and the metamaterials are captured by a linear elastic model. Sect. 4 presents the efficient simulation framework based on nonlinear finite element analysis that allows rational design optimization of the bending actuator. Sect. 5 shows the experimental results, and conclusions are drawn in Sect. 6.

2 Design concept

Pneumatic actuation technologies are widely used because air has low viscosity and permits rapid actuation. In this work, without loss of generality, we select a pneumatic rubber tube for actuation of the bending module, and as shown in Figure 1, the metamaterial structures envelop the rubber tube and tune the whole mechanical behavior of the coupled system. Due to the asymmetric distribution of the metamaterial structures, bending motions will be created upon pressurization.

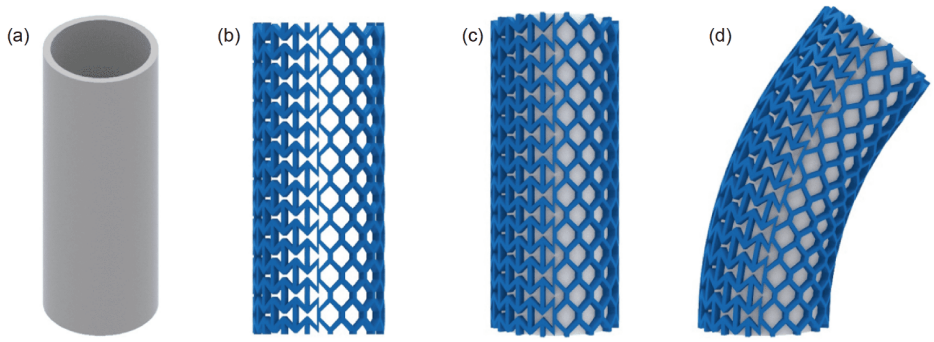

Figure 1 (Color online) Design concept of our method. (a) Rubber tube for actuation; (b) metamaterial structure combining auxetic and non-auxetic cells; (c) initial state and (d) a deformed state of the bending actuator.

We aim to maximize the bending motion by the rational design of the metamaterial structures. When the inner rubber tube is inflated, the cellular metamaterials are stretched in both the longitudinal direction and the circumferential direction. Herein, we employ metamaterial structures of positive Poisson's ratio (PPR) and negative Poisson's ratio (NPR), i.e., non-auxetic and auxetic materials, in order to transfer the induced circumferential strain to compressive and tensile axial strains, respectively, resulting in the desired bending motion.

The adopted geometries of PPR and NPR metamaterial structures are beam-like, which have been well used in many man-made materials and associated applications [27–29]. Their geometries can be described within the same frame using a set of parameters, as shown in Figure 2(a) and (b). It is noted that, since the metamaterial cells are thin-walled and their feature sizes are much smaller than the rubber tube, we may readily consider each cell to be a planar structure with a uniform width b and a uniform thickness t. The space each cell occupies is $w \times l$. In theory, the cells will attain the most pronounced effect of NPR (or PPR) when the feature size of gaps (or connecting bars between cells), denoted by g, vanishes. In practice, however, to avoid misconnection within a cell and ensure interconnections between neighboring cells, a small value of g is retained based on the experiments.

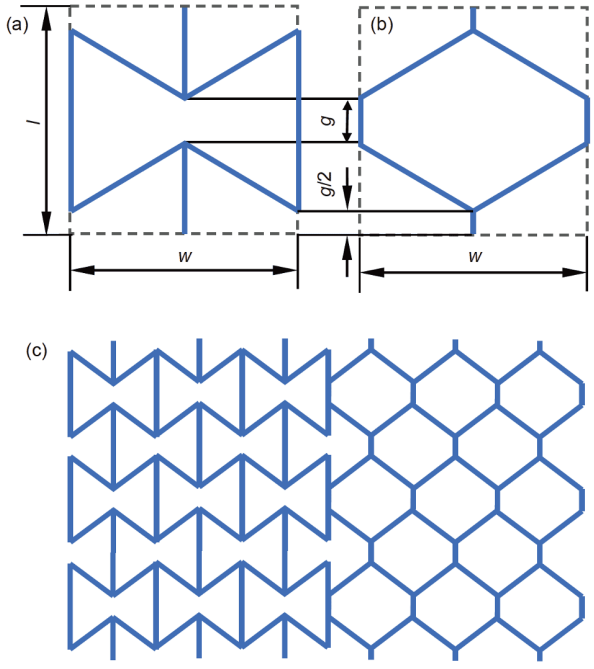

Figure 2 (Color online) Geometry layout of metamaterial structures. (a)–(b) Unit cells, and (c) their tessellations with direct interconnection.

The PPR and NPR metamaterial structures are symmetrically tessellated on the surface of the rubber tube, and these two different types of metamaterial structure can be naturally interconnected, as shown in Figure 2(c). We assume that the thin-walled rubber tube is of length L, radius R, and thickness T. There are m cells along the circumferential direction and n cells along the longitudinal direction. According to the geometry constraint, we have the relations:

$$L = ln, \tag{1}$$

$$2\pi R = mw. \tag{2}$$

3 Modelling

In this work, we adopt silicone rubbers to fabricate the actuation tube. Without loss of generality, we employ the generalized incompressible Neo-Hookean model to characterize the hyperelasticity of silicone rubber, with the free energy density w_r expressed by

$$w_r = \frac{\mu_r}{2}(\mathbf{I}_1 - 3), \tag{3}$$

where μ_r denotes the initial shear modulus, and $\mathbf{I}_1 = \mathrm{trace}(\mathbf{B})$ is the first invariant of strain invariants of the right Cauchy-Green deformation tensor $\mathbf{B} = \mathbf{F}^{\mathrm{T}} \cdot \mathbf{F}$ with $\mathbf{F}$ being the deformation gradient.

Based on some preliminary tests, we select Ecoflex 0030 as the rubber material, and the dog-bone shaped samples were tested by uniaxial tension experiments. The samples

each were stretched at a fixed rate of 300 mm/min, until 6 times its original length, as shown in the inset of Figure 3. Based on the experimental results of the force-displacement curve, we obtained the nominal stress and strain data.

We denote the stretch ratio of the lengthwise direction by λ, and the stretch ratios of the other two orthogonal directions in the cross-section of the samples are $1/\sqrt{\lambda}$, with the assumption that the silicone rubber is incompressible. Based on the strain energy density as defined in eq. (3), the nominal stress σ is

$$\sigma = \mu_r\left(\lambda - \frac{1}{\lambda^2}\right). \tag{4}$$

By comparing the experimental results and the theoretical predictions, the shear modulus was fitted to be $\mu_r = 0.05$ MPa for Ecoflex 0030 material, as shown in Figure 3.

For the material selection of metamaterial cells, we choose a type of commercially available polyurethane based silicone rubber, Hei-Cast 8400, which is made from three components, because of its good flow-ability and curing property. Moreover, the hardness of cured Hei-Cast 8400 can be flexibly varied by incorporating C component in the range of Shore 30A–90A, which provides a rich repertoire for material selection. The metamaterial structures are expected to be harder than the inner tube made of Ecoflex 0030 such that their networks can dominate the coupled structure to generate desired bending motions. In this sense, small strain will be induced in the metamaterial structures even at large displacements, and thus they are taken to be linear elastic materials.

To capture the geometry nonlinearity, we adopt the well-known Saint Venant-Kirchhoff model which is just an extension of the geometrically linear elastic material model to the geometrically nonlinear regime. The strain-energy density function for the Saint Venant-Kirchhoff model w_c is

$$w_c = \frac{\lambda_c}{2}[\mathrm{trace}(\mathbf{E})]^2 + \mu_c \mathrm{trace}(\mathbf{E}^2), \tag{5}$$

and $\mathbf{E}$ is the Lagrangian Green strain given by

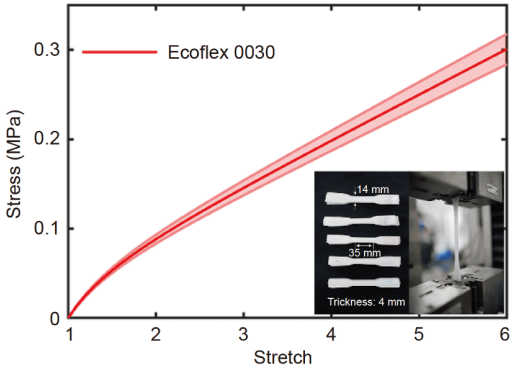

Figure 3 (Color online) Experiment stress-strain data and an incompressible neo-Hookean model for Ecoflex 0030.

$$\mathbf{E} = \frac{1}{2}(\mathbf{B} - \mathbf{I}), \tag{6}$$

where λ_c and μ_c are the Lamé constants that can be calculated from the Young's modulus E and the Poisson's ratio ν, and $\mathbf{I}$ is the second order unit tensor.

The dog-bone shaped samples of a series of Hei-Cast 8400 with different hardness (Shore 30A–90A) were fabricated and the uniaxial tension experiments were conducted. The samples were stretched at a fixed rate of 15 mm/min, and the largest stretch ratio reaches 5%, as shown in Figure 4. At small deformation, the stress and the strain exhibit an excellent linear relationship. The fitted Young's moduli turned out to be much larger than that of Ecoflex 0030, ranging from 1.15 to 19.45 MPa with the increase of hardness, as summarized in Table 1.

The bending actuator is a coupled system consisting of the rubber tube and surrounding cellular metamaterials. When the actuator undergoes large deformation upon pressurization, its state transits from the undeformed state to a deformed state which can be determined by balancing the strain energies of the two parts. By comparing their strain energies and considering the geometry profiles of the metamaterial cells, we identify two key dimensionless quantities for design:

$$\frac{l}{w}, \quad \frac{E}{\mu_r}.$$

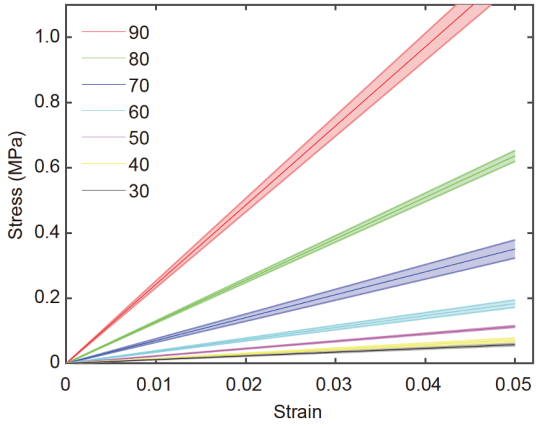

Figure 4 (Color online) The stress-strain relation for Hei-Cast 8400 of different hardness (Shore 30A–90A).

Table 1 Hardness and Young's modulus of Hei-Cast 8400

Shore hardness (A)	Young's modulus (MPa)
30	1.15
40	1.44
50	2.09
60	3.67
70	7.02
80	11.76
90	19.46

Specifically, the first term captures geometric profile of the metamaterial cell, while the second term captures the relative modulus of the metamaterial structures to the silicone rubber.

4 Simulation

The analysis of soft bodies composed of multimaterials has been challenging, due to the numerical issues that arise from the geometric nonlinearity, material nonlinearity, and the complex interplay between different materials [30,31]. These issues are usually characterized with mesh distortions at the regions of large strain and the interface of neighboring materials, which can hardly be fully addressed by a universal solution but can be alleviated by selecting appropriate mesh types and defining appropriate interaction constraints between different materials.

In our work, considering the inner rubber chamber is a thin-walled cylinder and the cellular metamaterials are beam-like members, we discretize them using shell elements and beam elements, respectively. Different from existing methods that delicately define their interactions using constraints (such as tie in Abaqus), we first build the metamaterial cells using beam elements, based on which we directly construct the mesh of the rubber tube, to readily form an integral part, without the need of defining cumbersome interactions. Besides, we encode python scripts within Abaqus to build complex customized models and automate the simulation process. This automated routing allows convenient modifications to our design by varying the parameters in the python scripts. The whole workflow of our simulation framework is shown in Figure 5, including the following steps:

(1) define the geometry and material parameters of the metamaterials in Matlab and write them into a python script;

(2) create the metamaterial cells in Abaqus based on the python script, using beam elements, and get the coordinate information of the nodes from the input file;

(3) obtain the connectivity relationship in Matlab between the mesh nodes based on Delaunay triangulation subdivision and send it back to Abaqus;

(4) define shell elements based on connectivity relations to construct the inner chamber, accomplish the nonlinear analysis and obtain the displacement field;

(5) calculate the bending angle from the analysis results.

The fixed parameters are provided in Table 2. Considering the manufacturing constraint, the number of metamaterial cells in the circumferential direction is set to be $m = 16$ while the number of cells in the longitudinal direction is determined by the aspect ratio of the cell which is subject to design optimization. The internal pressure is applied directly on the constructed closed shell elements, which correspond to the side surface of the chamber and the covers on the end faces. To prevent possible rupture, we limit the largest internal pressure smaller than 0.03 MPa. The two covers on the end faces are set to be rigid bodies by coupling the motions on the cover plane. The bottom cover is fixed while the top cover works freely as an end-effector. The bending angle refers to the angle of top cover relative to the bottom cover.

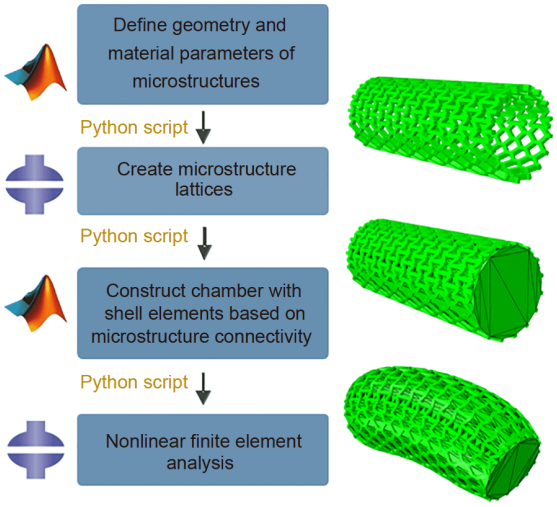

Figure 5 (Color online) The whole workflow of the simulation framework.

The geometry ratio and the material ratio are independently controlled for parametric optimization. According to eq. (1) and eq. (2), the dimensionless geometry aspect ratio can be expressed by

$$\frac{l}{w} = \frac{mL}{2n\pi R}. \tag{7}$$

Considering the fixed parameters in Table 2, we have the relation that the geometry ratio of the metamaterial structure is inversely directly proportional to the number of cells along the lengthwise direction, i.e., $\frac{l}{w} \propto \frac{1}{n}$. The other parameter $\frac{E}{\mu_r}$ is inversely directly proportional to E, with μ_r being fixed. Thus, the variations of the geometry ratio and material ratio translate into variations of n and E, respectively. By changing their values under a given internal pressure, the bending angle varies accordingly, as shown in Figure 6. The number of cells in the longitudinal direction n ranges from 6 to 12 with a step of 1, while the Young's modulus of the metamaterials E ranges from 4 MPa to 20 MPa with a step of

Table 2 Parameters setting in the simulation and experiments

Parameter	L	R	m	T	t	b	T	μ_r	v
Value	80 mm	15 mm	16	2.2 mm	2.00 mm	1.3 mm	3 mm	0.05 MPa	0.35

1 MPa.

Figure 6 shows that the bending angle depends greatly on the geometry ratio and the material ratio, for different levels of pressurization. For the internal pressure of 0.005, 0.015 and 0.030 MPa, the optimal material ratios are 100, 100 and 142, respectively, while the optimal geometry ratios are 1.94 (n = 7), 1.70 (n = 8) and 1.70 (n = 8), respectively. Besides, large bending motions are achieved. For P = 0.030 MPa, the maximal bending angle reaches up to 45.4°. Figure 7 shows the deformed states of some cases for different pressures and material properties of metamaterial, with n = 8.

5 Experiment

The presented design concept was validated by experiments. We select the optimal design for prototyping, i.e., the case in Figure 7(g), with the metamaterial hardness 70A and n = 8. The cellular metamaterials were manufactured by 3D printing techniques and the rubber chamber was manufactured by molding and casting. The chamber's end faces were closed by two rigid covers. The metamaterial structures, the rubber tube and the covers were glued together to form an airtight actuator prototype.

A pneumatic control system was designed and constructed to trigger the actuator's bending deformation. The pressurized air was produced by an air compressor (2X950-50; OUTSTANDING). To regulate output pressure, an electronic proportional valve (ITV2050-312BL; SMC) was controlled by PWM signals of the microcontroller (Arduino Nano; Arduino). A pressure calibrator (BOOST.CPM.0103; BOOST Instrument Tech) recorded the input pressure of the

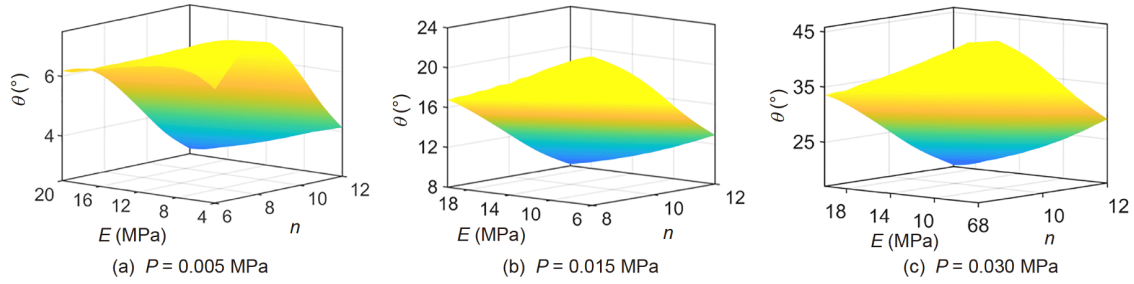

Figure 6 (Color online) The relationship between the bending angle with the geometry ratio and material ratio under different pressures.

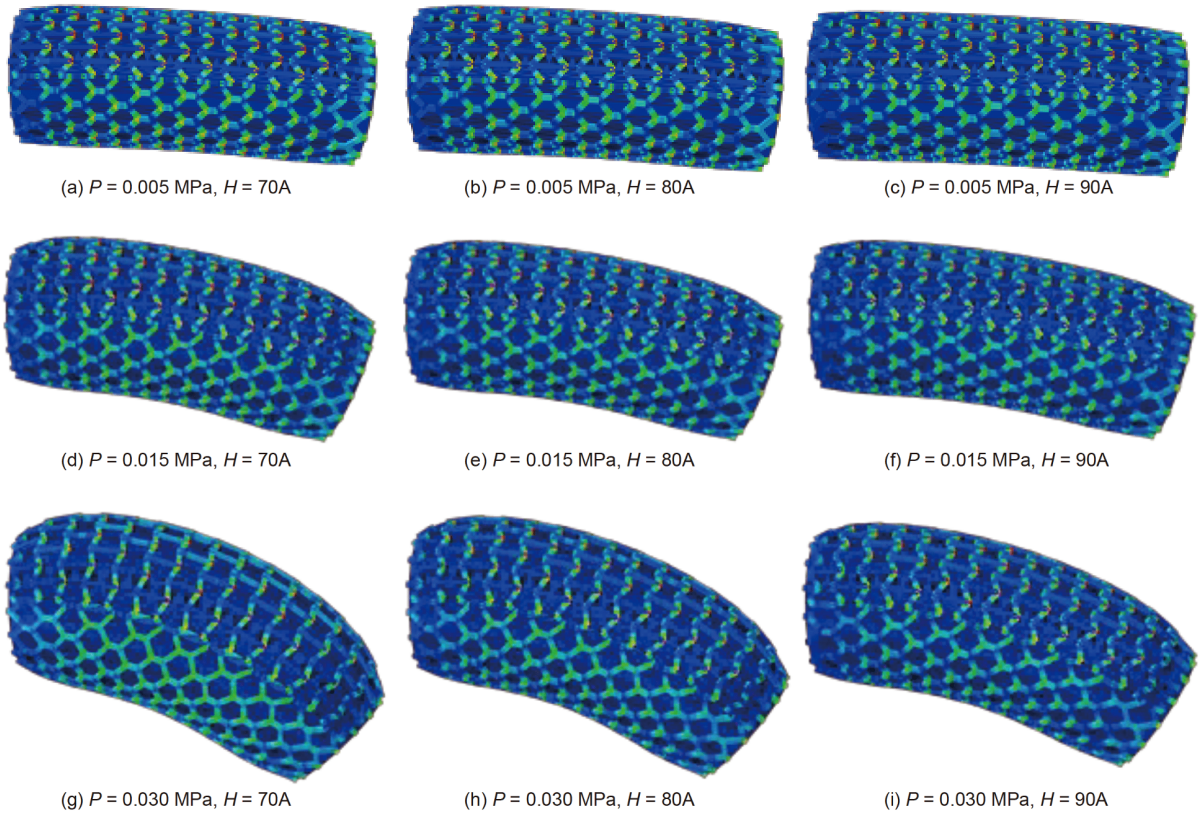

Figure 7 (Color online) Some simulation cases for different internal pressures P and material hardness of metamaterial structure H, with n = 8.

actuator. All programs were performed in Matlab which communicated with the Arduino Nano board. The pressure was increased slowly to ensure a quasi-static process.

With the increase of the internal pressure, the differential elongation of the auxetic and the non-auxetic materials arises, leading the actuator to bend significantly. The global bending deformation was recorded by a digital camera (Sony FE90F2.8). Figure 8 shows the bending states of three cases (Shore 70A, 80A, 90A) under different pressures ranging from 0 to 0.025 MPa. With the increase of inner pressure, the actuator made of Shore 70A materials exhibits the ballooning effect, which in some cases may be undesired. With the increase of Young's modulus of metamaterials E, the critical pressure that triggers obvious ballooning effects also increases. For actuators of Shore 80A and 90A, the ballooning effect is well suppressed.

Figure 9 shows the comparison of the simulation result and the experimental result. The global bending angle and the pressure exhibit an excellent linear relationship, making it convenient for control in practical applications. The optimal experimental angle is approximately 34° under P = 0.025 MPa. The ratio of the angle to the length is 0.43°/mm and is much larger than the latest reported counterpart, 0.18°/mm in ref. [26]. The experimental results are well in line with the simulation, with a deviation of less than 10%.

Besides the errors of measurement, deviations may arise from the gravity of the actuator and the viscoelasticity of the materials which were not taken into account in this work.

(a) P = 0 MPa, H = 70A (b) P = 0.005 MPa, H = 70A (c) P = 0.010 MPa, H = 70A (d) P = 0.015 MPa, H = 70A (e) P = 0.020 MPa, H = 70A (f) P = 0.025 MPa, H = 70A

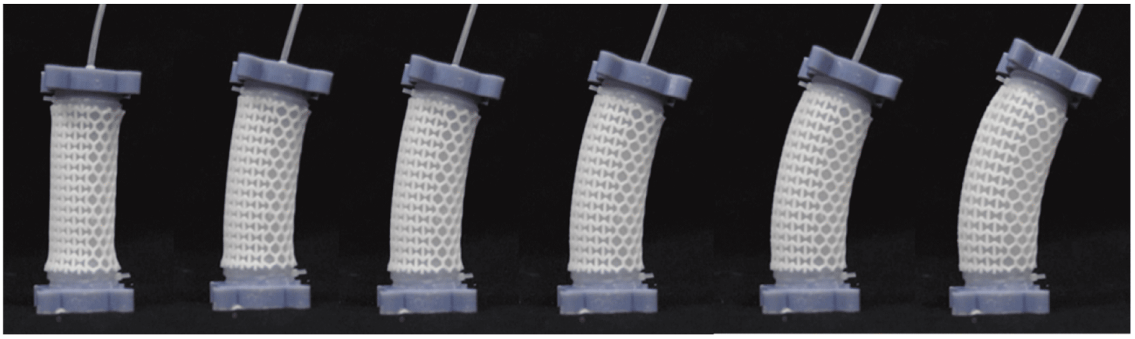

(g) P = 0 MPa, H = 80A (h) P = 0.005 MPa, H = 80A (i) P = 0.010 MPa, H = 80A (j) P = 0.015 MPa, H = 80A (k) P = 0.020 MPa, H = 80A (l) P = 0.025 MPa, H = 80A

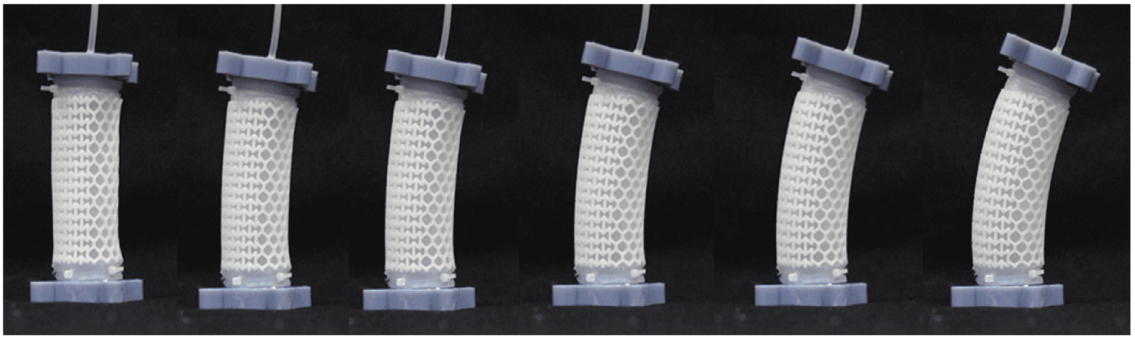

(m) P = 0 MPa, H = 90A (n) P = 0.005 MPa, H = 90A (o) P = 0.010 MPa, H = 90A (p) P = 0.015 MPa, H = 90A (q) P = 0.020 MPa, H = 90A (r) P = 0.025 MPa, H = 90A

Figure 8 (Color online) Deformed states of the bending actuator under pressures from 0 to 0.025 MPa, for Hei-Cast 8400 (Shore 70A, 80A and 90A).

There is still room for improvement in design and manufacture. Currently, the size of auxetic and non-auxetic metamaterial cells is greatly limited by the resolution of 3D printing, and thus we limit the number of cells along the circumferential direction to be 16. With the improving capabilities of manufacturing soft elastomers with smaller feature sizes [32,33], we believe that the design can be further improved to exploit the potential of metamaterials for innovative design of soft actuators and manipulators [12,34].

We also conduct blocking force tests to evaluate the load capacity of the bending actuators, as shown in Figure 10. The actuator was fixed at one end and its other end was connected to the force sensor (K3D120; ME-Messsysteme). Figure 10 (b) shows that the blocking force increases with the applied pressure ranging from 0 to 0.025 MPa. The actuator made of Hei-Cast 8400 (Shore 70A) achieves the largest blocking force up to 1.3 N.

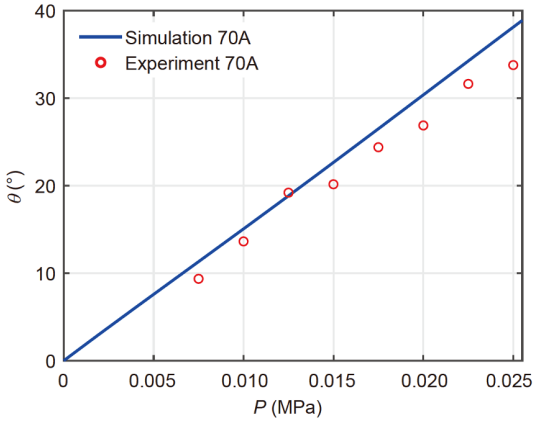

Figure 9 (Color online) The simulation and experimental bending angle under different pressure for Hei-Cast 8400 (Shore 70A) and n=8.

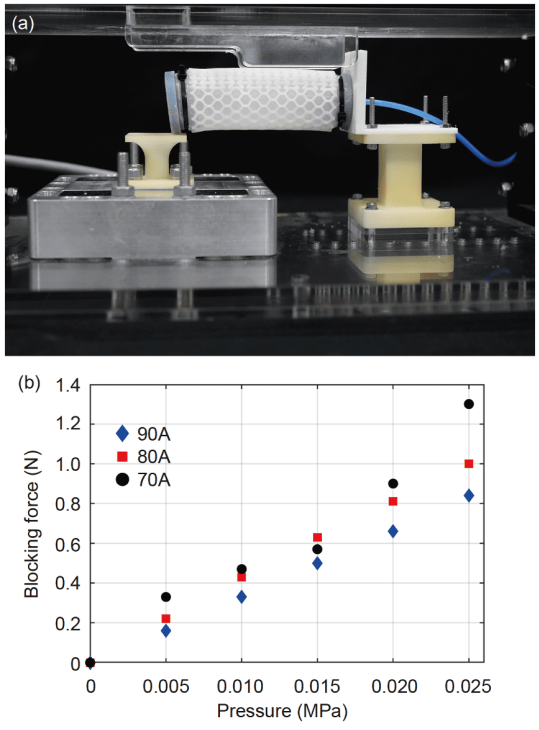

Figure 10 (Color online) Blocking force test of the bending actuators. (a) Experiment platform; (b) experimental results.

6 Conclusions

In this paper, we provide an alternative solution to soft bending actuators, with advantages of compact design, large bending motion, and convenient fabrication. To provide insight into the design optimization, we develop a computation framework by constructing metamaterial structures and the inner chamber as an integral part that allows efficient simulation of the coupled system under pressurization. This simulation framework leads to rational design optimization by varying the geometry ratio and the material ratio of the bending actuator to generate the maximal bending motion. The design concept was well validated through experiments. A remarkable bending angle of 34° (0.43°/mm) and a blocking force of 1.3 N were achieved under an actuation pressure of 0.025 MPa.

Our design framework is readily applicable to general beam-like metamaterial cells. In the future, we hope to incorporate more kinds of metamaterials to program complex motions of soft actuators and robots, such as twisting. By exploring the vast design space offered by the metamaterials, a large variety of soft robotic applications are to be unlocked.

This work was supported by the National Natural Science Foundation of China (Grant No. 51905340), and the Shanghai Sailing Program (Grant No. 19YF1422900).

1 Rus D, Tolley M T. Design, fabrication and control of soft robots. Nature, 2015, 521: 467–475
2 Davis S, Caldwell D G. Braid effects on contractile range and friction modeling in pneumatic muscle actuators. Int J Robotics Res, 2006, 25: 359–369
3 Polygerinos P, Wang Z, Galloway K C, et al. Soft robotic glove for combined assistance and at-home rehabilitation. Robotics Autonomous Syst, 2015, 73: 135–143
4 Ge L, Chen F, Wang D, et al. Design, modeling, and evaluation of fabric-based pneumatic actuators for soft wearable assistive gloves. Soft Robotics, 2020
5 Osborn L E, Dragomir A, Betthauser J L, et al. Prosthesis with neuromorphic multilayered e-dermis perceives touch and pain. Sci Robot, 2018, 3: eaat3818
6 Liang Z, Cheng J, Zhao Q, et al. High-performance flexible tactile sensor enabling intelligent haptic perception for a soft prosthetic hand. Adv Mater Technol, 2019, 4: 1900317
7 Hawkes E W, Blumenschein L H, Greer J D, et al. A soft robot that navigates its environment through growth. Sci Robot, 2017, 2: eaan3028
8 Zhang J, Wang T, Wang J, et al. Dynamic modeling and simulation of inchworm movement towards bio-inspired soft robot design. Bioinspir Biomim, 2019, 14: 066012
9 Cao J, Liang W, Ren Q, et al. Modelling and control of a novel soft crawling robot based on a dielectric elastomer actuator. In: Proceed-

ings of the 2018 IEEE International Conference on Robotics and Automation (ICRA). IEEE, 2018. 1–9

10 Yang Y, Chen Y, Li Y, et al. Bioinspired robotic fingers based on pneumatic actuator and 3D printing of smart material. Soft Robotics, 2017, 4: 147–162

11 Chen F, Xu W, Zhang H, et al. Topology optimized design, fabrication, and characterization of a soft cable-driven gripper. IEEE Robot Autom Lett, 2018, 3: 2463–2470

12 Calisti M, Giorelli M, Levy G, et al. An octopus-bioinspired solution to movement and manipulation for soft robots. Bioinspir Biomim, 2011, 6: 036002

13 Ilievski F, Mazzeo A D, Shepherd R F, et al. Soft robotics for chemists. Angew Chem, 2011, 123: 1930–1935

14 Yang C, Kang R, Branson D T, et al. Kinematics and statics of eccentric soft bending actuators with external payloads. Mechanism Machine Theor, 2019, 139: 526–541

15 Galloway K C, Polygerinos P, Walsh C J, et al. Mechanically programmable bend radius for fiber-reinforced soft actuators. In: Proceedings of the 2013 16th International Conference on Advanced Robotics (ICAR) [Internet]. Montevideo, Uruguay: IEEE, 2013. 1–6

16 Wang Z, Polygerinos P, Overvelde J T B, et al. Interaction forces of soft fiber reinforced bending actuators. IEEE/ASME Trans Mechatron, 2017, 22: 717–727

17 Elsayed Y, Vincensi A, Lekakou C, et al. Finite element analysis and design optimization of a pneumatically actuating silicone module for robotic surgery applications. Soft Robotics, 2014, 1: 255–262

18 Hiller J, Lipson H. Automatic design and manufacture of soft robots. IEEE Trans Robot, 2012, 28: 457–466

19 Chen F, Liu K, Wang Y, et al. Automatic design of soft dielectric elastomer actuators with optimal spatial electric fields. IEEE Trans Robot, 2019, 35: 1150–1165

20 Zhang H, Wang M Y, Chen F, et al. Design and development of a soft gripper with topology optimization. In: Proceedings of the 2017 IEEE/RSJ International Conference on Intelligent Robots and Systems (IROS). IEEE, 2017. 6239–6244

21 Zhang H, Kumar A S, Chen F, et al. Topology optimized multimaterial soft fingers for applications on grippers, rehabilitation, and artificial hands. IEEE/ASME Trans Mechatron, 2018, 24: 120–131

22 Rafsanjani A, Bertoldi K, Studart A R. Programming soft robots with flexible mechanical metamaterials. Sci Robot, 2019, 4: eaav7874

23 Mark A G, Palagi S, Qiu T, et al. Auxetic metamaterial simplifies soft robot design. In: Proceedings of the 2016 IEEE International Conference on Robotics and Automation (ICRA) [Internet]. Stockholm: IEEE. 2016. 4951–4956

24 Goswami D, Liu S, Pal A, et al. 3D-architected soft machines with topologically encoded motion. Adv Funct Mater, 2019, 29: 1808713

25 Han Y, Lu W. Optimizing the deformation behavior of stent with nonuniform Poisson's ratio distribution for curved artery. J Mech Behav BioMed Mater, 2018, 88: 442–452

26 Hasse A, Mauser K. Poisson induced bending actuator for soft robotic systems. Soft Robotics, 2020, 7: 155–167

27 Lakes R. Foam structures with a negative Poisson's ratio. Science, 1987, 235: 1038–1040

28 Bertoldi K, Reis P M, Willshaw S, et al. Negative Poisson's ratio behavior induced by an elastic instability. Adv Mater, 2010, 22: 361–366

29 Babaee S, Shim J, Weaver J C, et al. 3D soft metamaterials with negative Poisson's ratio. Adv Mater, 2013, 25: 5044–5049

30 Lipson H. Challenges and opportunities for design, simulation, and fabrication of soft robots. Soft Robotics, 2014, 1: 21–27

31 Duriez C, Bieze T. Soft robot modeling, simulation and control in real-time. In: Laschi C, Rossiter J, Iida F, et al, eds. Soft Robotics: Trends, Applications and Challenges [Internet]. Cham: Springer International Publishing, 2017. 103–109

32 Truby R L, Lewis J A. Printing soft matter in three dimensions. Nature, 2016, 540: 371–378

33 Wallin T J, Pikul J, Shepherd R F. 3D printing of soft robotic systems. Nat Rev Mater, 2018, 3: 84–100

34 Wu J, Wang J, Wang L, et al. Dynamics and control of a planar 3-DOF parallel manipulator with actuation redundancy. Mechanism Machine Theor, 2009, 44: 835–849